ToRoS: A Topology Optimization Approach for Designing Robotic Skins

JUAN MONTES MAESTRE, ETH Zürich, Switzerland
RONAN HINCHET, ETH Zürich, Switzerland
STELIAN COROS, ETH Zürich, Switzerland
BERNHARD THOMASZEWSKI, ETH Zürich, Switzerland

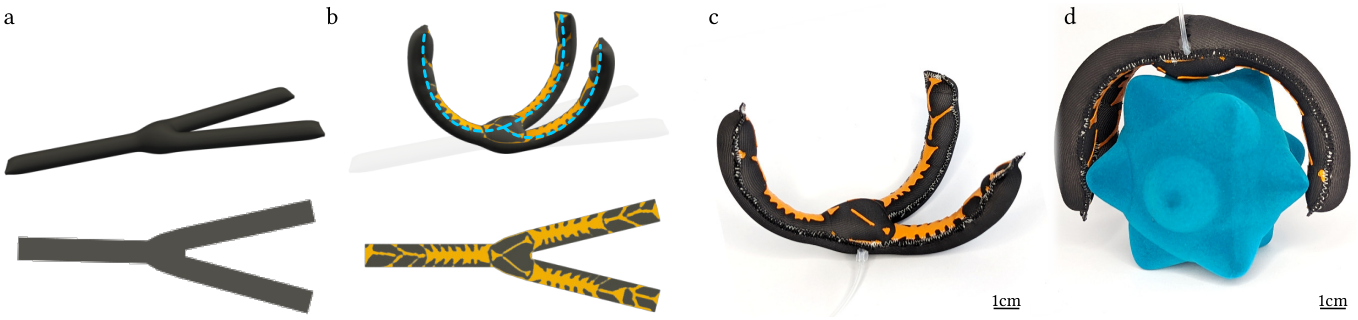

Fig. 1. Automated design of a pneumatic gripper using our method. An initial design (*a*, *bottom*) fails to produce the target deformation (*blue*) when inflated (*top*). Our method produces an optimized reinforcement pattern (*b*, *bottom*) such that the inflated shape (*top*) closely approximates the target deformation. A physical prototypes (*c*) reproduces the predicted deformation, allowing it to grasp and lift an object conforming to the target shape (*d*).

Soft robotics offers unique advantages in manipulating fragile or deformable objects, human-robot interaction, and exploring inaccessible terrain. However, designing soft robots that produce large, targeted deformations is challenging. In this paper, we propose a new methodology for designing soft robots that combines optimization-based design with a simple and cost-efficient manufacturing process. Our approach is centered around the concept of robotic skins—thin fabrics with 3D-printed reinforcement patterns that augment and control plain silicone actuators. By decoupling shape control and actuation, our approach enables a simpler and cost-efficient manufacturing process. Unlike previous methods that rely on empirical design heuristics for generating desired deformations, our approach automatically discovers complex reinforcement patterns without any need for domain knowledge or human intervention. This is achieved by casting reinforcement design as a nonlinear constrained optimization problem and using a novel, three-field topology optimization approach tailored to fabrics with 3D-printed reinforcements. We demonstrate the potential of our approach by designing soft robotic actuators capable of various motions such as bending, contraction, twist, and combinations thereof. We also demonstrate applications of our robotic skins to robotic grasping with a soft three-finger gripper and locomotion tasks for a soft quadrupedal robot.

CCS Concepts: • **Applied computing** → **Computer-aided manufacturing**; • **Computing methodologies** → *Modeling and simulation.*

Authors' addresses: Juan Montes Maestre, ETH Zürich, Switzerland, jmontes@inf.ethz.ch; Ronan Hinchet, ETH Zürich, Switzerland, ronanhinchet@gmail.com; Stelian Coros, ETH Zürich, Switzerland, stelian@inf.ethz.ch; Bernhard Thomaszewski, ETH Zürich, Switzerland, bthomasz@ethz.ch.

0730-0301/2023/12-ART $15.00
https://doi.org/10.1145/3618382

ACM Reference Format:
Juan Montes Maestre, Ronan Hinchet, Stelian Coros, and Bernhard Thomaszewski. 2023. ToRoS: A Topology Optimization Approach for Designing Robotic Skins. *ACM Trans. Graph.* 42, 6 (December 2023), 11 pages. https://doi.org/10.1145/3618382

1 INTRODUCTION

The emergence of soft robotics has given rise to a large and diverse range of robots that, in many ways, surpass the limitations of their rigid counterparts. Their soft structure provides unique advantages when it comes to robotic manipulation of fragile or deformable objects, human-robot interaction, and even exploration of otherwise inaccessible terrain. Regardless of their application, soft robots must produce targeted deformations for functioning. While there are many different approaches [El-Atab et al. 2020], pneumatic actuation remains the most widely used option [Rus and Tolley 2015]. Several ways of controlling the inflated shape of pneumatic actuators have been explored. One approach is to adjust the shape of internal air chambers embedded in a volumetric silicone matrix [Shepherd et al. 2011]. Another option is to structure plain actuators made from synthetic rubber membranes with strain-limiting materials such as fibers [Bishop-Moser et al. 2012; Hirai et al. 2000] or sheets [Mosadegh et al. 2014; Sun et al. 2013] that can bend but not stretch. While these existing approaches can produce reasonable results, they rely on expert designers and trial-and-error strategies with physical prototypes.

In this work, we propose a novel computational approach for creating soft robots that combines optimization-based design with a simple and cost-efficient manufacturing process. We decouple shape control and actuation by augmenting plain silicone actuators with robotic skins—thin, stretchable fabrics structured with flexible, 3D-printed reinforcements. Our robotic skins enable an entirely planar fabrication process, thus greatly reducing manufacturing

complexity. The central challenge, then, is to find reinforcement layouts that lead to desired deformations upon inflation. While topology optimization is a natural choice in this setting, we show through examples that conventional methods perform poorly and fail to generate useful designs. Specific problems include checker boarding artifacts, non-binary solutions, and islands of material that are difficult to manufacture. To address these problems, we propose a topology optimization approach tailored to the specific challenges of robotic skin design, including geometric nonlinearities, complex material behavior, as well as manufacturing constraints. Our approach builds on a so called three-field formulation that builds smoothing, filtering for minimum thickness, and material binarity directly into the optimization process. We furthermore introduce a new perimeter penalty that identifies and eliminates material islands, which improves both manufacturability and performance. Finally, whereas conventional methods require the user to prescribe a material budget, our method does not impose such constraints and thus enjoys more flexibility in finding designs that best approximate performance goals.

We demonstrate the potential of our approach on a series of examples including reinforced fabrics with desired macromechanical properties and soft actuators that can bend, twist, and contract. We further show applications to robotic grasping with a soft three-finger gripper and locomotion tasks for a soft quadrupedal robot. To validate the feasibility of our simulation results, we build and evaluate physical prototypes for all our designs.

2 RELATED WORK

Designing soft actuators and robots is a problem that overlaps with several active fields of research in the graphics and robotics communities. We review the most immediately related works below.

Designing Soft Robots. Soft robots are structures made of flexible materials with the aim of mimicking living organisms. In comparison to conventional robots made of rigid materials, they provide greater flexibility for deformation at the cost of increased design complexity. While many strategies for actuating soft mechanisms exist, including shape-memory alloys [Buckner et al. 2020], cables [Bern et al. 2017] and magnets [Zou et al. 2018], pneumatic actuation is arguably the most widely used option. Regardless of the mechanism used, controlling the deformations resulting from actuation is a challenging problem. To this end, [Grossi et al. 2021] mimic caterpillar locomotion by pressurizing auxetic structures, [Bern et al. 2017; Min et al. 2019] find optimal routing of muscle fibers to achieve desired deformations and [Buckner et al. 2020] enrich textiles with actuation and sensing abilities. The medium in which the device operates opens new challenges. [Ma et al. 2021] find controllers for swimmer robots and [Branyan et al. 2022] modulate friction such as to mimick the locomotion pattern of snakes. For a more comprehensive review on soft robot design we refer to Pinskier and Howard [2022].

Active Robotic Skins. Closer to our work, a variety of methods aim to provide multiple functionalities to a single device. Shah et al. [2021] design robotic structures that can change their shape such as to adapt to changes in their environment. Using the same design for multiple gaits, Shepherd et al. [2011] control the motion of a pneumatic crawler by changing the topology of its internal channels. Zou et al. [2018] emulate the motion of a caterpillar by rearranging a set of chambered magnets. Case et al. [2019] use the concept of robotic skins, where the actuation of a device is driven by a replaceable *skin* worn by a passive structure. Different skins allow a single structure to implement multiple functionalities. Booth et al. [2018] demonstrates this concept for soft-memory alloys and pneumatic devices. While the aforementioned works rely on manual design, we propose an automated approach to designing robotic skins via topology optimization.

Computational Design for Deformation. Controlling deformations that result from internal actuation is a core capability for soft robotics applications. With the widespread availability of 3D printers, designing materials that deform into desired shapes has moved into the focus of the graphics community. One line of work explores the use of multimaterial printers for this purpose [Bickel et al. 2010; Skouras et al. 2012; Zehnder et al. 2017] while others rely on microstructures to modulate macromechanical properties [Panetta et al. 2015; Schumacher et al. 2015, 2018; Tricard et al. 2020; Zhu et al. 2017]. Using the concept of structured fabrics, Jordan et al. [2020] print reinforcement patterns to encode desired curvature into pre-stretched textiles. Similarly, Montes et al. [2023] optimize for stripe-shaped reinforcement patterns to control the mechanical response of reinforced fabrics. While stripe patterns are tailored to high-stiffness-ratio materials—compliant in one direction, stiff in the orthogonal one—the design space of our topology optimization approach is much larger, providing the flexibility needed to discover complex designs for functioning soft robots.

Inflatables with Desired Shapes. A number of graphics works has investigated the design of pneumatic structures. For example, Skouras et al. [2012] optimize for rest shapes of silicone balloons that inflate into desired shapes. Follow up work from the same group considered the design of inflatable structures made from planar patterns of inextensible material [Skouras et al. 2014]. Another line of work has focused on controlling inflatables with metamaterial designs such as kirigami [Branyan et al. 2022; Jin et al. 2020]. Panetta et al. [2021] compute channels that, when pressurized, deploy into desired shapes.

Fabricating Pneumatic Actuators. Manufacturing soft robots and actuators is a challenging task, often involving multiple steps, materials, and processes; see, e.g., Schmitt et al. [2018] for an overview. Digital manufacturing technologies such as 3D printing can automate these tasks, and consequently greatly increase design possibilities [Tawk and Alici 2021; Wallin et al. 2018; Yirmibesoglu et al. 2018]. However, existing processes require complex and specialized 3D-printing setups to create multi-material distributions [Byrne et al. 2018; Coulter and Ianakiev 2015; Schaffner et al. 2018]. In addition, 3D printing of ultra-soft elastic materials is still in its infancy. An alternative approach to manufacturing reinforced plain actuators is to separately fabricate a soft elastic bladder [Shepherd et al. 2011] and 3D printed reinforcements, and then assemble them [Baumgartner et al. 2020; Chen et al. 2021a]. Such actuators are simple to

manufacture but assembling reinforcement structures can be difficult and cumbersome. Techniques to ease reinforcement assembly on inflatables include heat transfer [Nguyen and Zhang 2020] and selective cutting [Pikul et al. 2017]. Sewing reinforcing components together is another option [Yap et al. 2017] and programmable knitting machines [Luo et al. 2022] can be used to integrate reinforcing fibers into fabrics. While all these strategies are promising, they remain complex and constrain design options in terms of shape and materials.

Topology Optimization. Topology optimization has become an important tool in the design of structures that are stiff but lightweight [Allaire et al. 2005, 2004; Andreassen et al. 2011; Bendsøe and Sigmund 1995; Bendsoe and Sigmund 2013; Zehnder et al. 2021]. While most works have focused on linear problems, another line of research has studied nonlinear topology optimization for finite deformation problems. Kemmler et al. [2005] tackle the problem of instabilities related to buckling using a geometrically nonlinear approach. Caasenbrood et al. [2020] propose a computational framework for designing pressure-driven soft robots using nonlinear topology optimization. Recent work by Chen et al. [2021b] likewise used topology optimization to design skeletons for soft bladders such as to best approximate given displacement targets. While their method leads to three-dimensional designs that are fabricated using custom-made molds, the two-dimensional patterns generated by our approach can be printed directly onto the fabric substrate. As another key difference, the method by Chen et al. [2021b] produces designs for user-prescribed material budget and pressure, whereas our approach automatically determines optimal values for these parameters.

A central problem of topology optimization is to deal with low-density elements that are prone to large distortions. Wang et al. [2014] address low stiffness problems that arises in nonlinear topology optimization with an energy-interpolation approach that uses a linear material model for low-density elements. Our method does not suffer from such problems since the textile substrate automatically regularizes low stiffness regions. However, our setting introduces the new challenge of isolated material islands that are hard to manufacture. Whereas such disconnected components do not appear in gravity-regularized problems that seek filled-void material assignments, our fabric-reinforcement material distributions are prone to such artefacts. We address this problem using a three-field topology optimization approach with a novel perimeter regularizer that eliminates these artefacts.

Perimeter Control in Topology Optimization. Several works have used descriptions of the perimeter as a tool to constrain the shape of the optimized design. In his work, Sigmund [2007] noted that the perimeter of a design could be extracted by eroding a design and subtracting it from the original design. Luo et al. [2019] used this idea to identify the interface of a shell. In contrast, our work penalizes the perimeter in order to discourage unnecessary additions of material.

3 COMPUTATIONAL MODEL

The goal of our method is to compute reinforcement patterns for textile panels that, when assembled and pressurized, produce a prescribed deformation. Fig. 2 shows a high-level overview of our automated design loop. Starting from a random density field (Fig. 2a), we compute its deformation under static equilibrium (Fig. 2b), perform sensitivity analysis to find the gradient (Fig. 2c), and update the mesh density of the design (Fig. 2d). We use three-field topology optimization along with the perimeter regularizer to generate manufacturable designs (Fig. 2e). We describe each of these steps in the following.

3.1 Forward Simulation

Our robotic skins are 3D printed reinforcements on thin layers of fabric, motivating us to model them as discrete shells made of linear triangular elements. Pneumatic devices experience extreme deformations involving a complex mechanical response that requires accurate material modeling. To this end, we perform a characterization of the fabric (Fig. 3), which demonstrates that it shows an initial linear stress-strain behavior followed by a sudden exponential stiffening. We model this phenomenon by fitting a hyper-elastic material based on Gent's model [Gent 1996]. The strain energy density function is given per-element (e) as

$$\begin{aligned}\psi^e_{\text{stretch}}(\lambda_1,\lambda_2) = &-\mu(c_1-1)^2\ln\left(1-\frac{(\lambda_1-1)^2}{(c_1-1)^2}\right)\\ &-\mu(c_1-1)^2\ln\left(1-\frac{(\lambda_2-1)^2}{(c_1-1)^2}\right)\\ &-\frac{\lambda}{2}(c_2-1)^2\ln\left(1-\frac{(\lambda_1+\lambda_2-2)^2}{(c_2-1)^2}\right),\end{aligned} \tag{1}$$

where λ_1 and λ_2 are the principal stretches of the Biot strain tensor $\mathbf{B} = \sqrt{\mathbf{F}^T\mathbf{F}}$ and $\mathbf{F} = \frac{\partial \boldsymbol{x}}{\partial \bar{\boldsymbol{x}}}$ is the 3×2 deformation gradient relating the deformed configuration of the shell $\boldsymbol{x}$ to the undeformed configuration $\bar{\boldsymbol{x}}$ given by flat patterns. Furthermore, λ and μ describe the Lamé parameters, whereas c_1 and c_2 determine the shape of the log barrier. This material can be viewed as a St.Venant-Kirchhoff (StVK) model augmented with a logarithmic barrier. Indeed, for values of c_1 and c_2 approaching infinity, the energy density function converges to the standard StVK solid. We fit these parameters to experimental data obtained from uniaxial stretch experiments (Sec. 4.2). As shown in Fig. 3, the resulting model closely tracks the measured behavior of the real fabric for deformations up to 180%. As an additional benefit, the log barrier acts as a regularizer for designs with sparse reinforcement distributions, preventing the pressure energy from overcoming the elastic energy of the fabric.

We assign materials on a per-element (e) basis through linear interpolation of the fitted Lamé parameters of the textile (λ_{textile},μ_{textile}) and reinforcement ($\lambda_{\text{reinforcement}}$,$\mu_{\text{reinforcement}}$) materials as

$$\lambda^e = (1-\rho^e)\lambda_{\text{fabric}} + \rho^e\lambda_{\text{reinforcement}} \text{ and} \tag{2}$$

$$\mu^e = (1-\rho^e)\mu_{\text{fabric}} + \rho^e\mu_{\text{reinforcement}}, \tag{3}$$

where $\boldsymbol{\rho}$ defines a density field that describes the density distribution of reinforcement material.

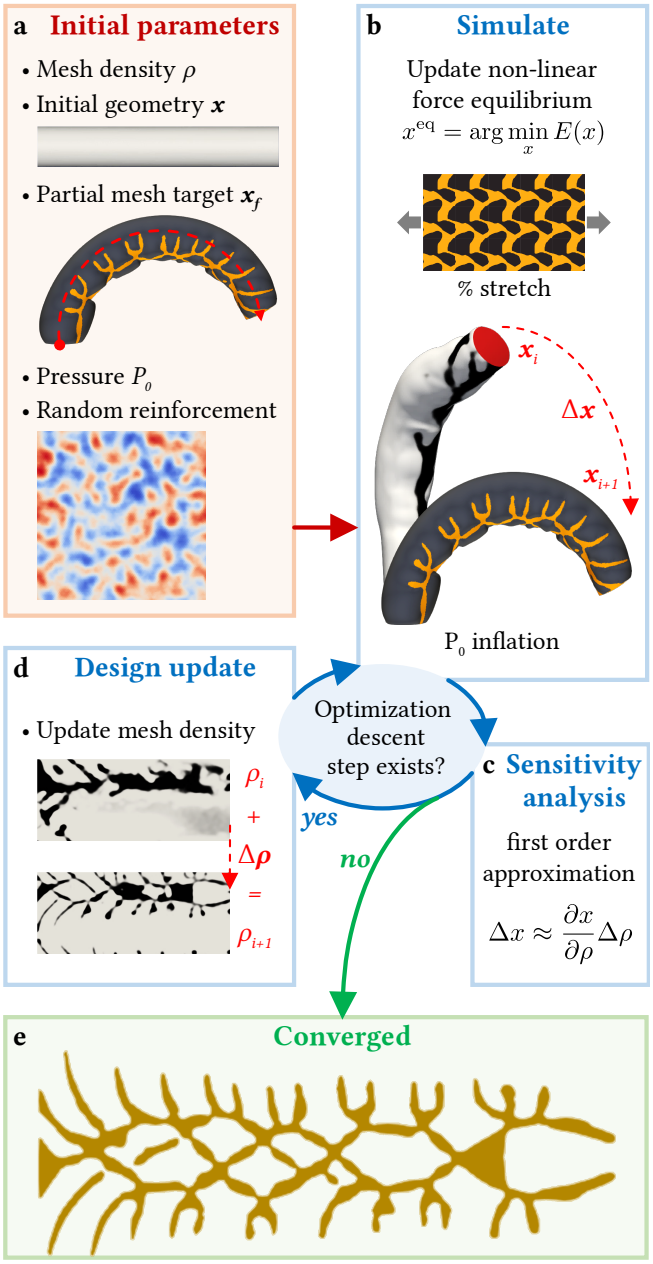

Fig. 2. Simulation and topology optimization workflow. Given initial parameters and a target shape (*a*), our automated design loop repeats three steps. First, the inflated shape for the current design is simulated (*b*). Second, sensitivity analysis is used to evaluate the gradient of the design objective wrt. per-element material parameters (*c*). Third, this gradient is used to compute an update for material parameters (*d*). The converged design is manufactured (*e*).

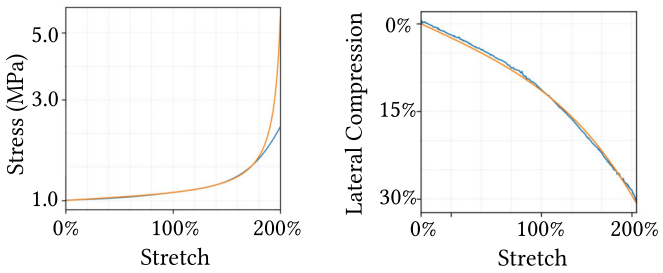

Fig. 3. Hyper-elastic material for the textile fitted (orange) from uni-axial stretch data (blue). The fitted parameters lead to accurate stresses (*left*) and lateral compression (*right*) for up to 180% stretch.

Bending energy. Since our parameterization defines different materials per element, we discretize the curvature operator using the triangle-averaged model by Grinspun et al. [2006], allowing us to use per-triangle material properties to compute bending stiffness. The curvature operator is computed for every triangle as the sum of the contributions of each edge i of the triangle as

$$\Lambda_e = \sum_i \frac{\theta_i}{2\bar{A}\bar{l}_i} \bar{\boldsymbol{t}}_i \bar{\boldsymbol{t}}_i^T, \tag{4}$$

where θ_i is the average signed angle of the normals of the triangles neighboring the edge in the deformed configuration. The remaining quantities are computed in the undeformed configuration, with $\bar{A}$ corresponding to the area of the triangle, $\bar{l}_i$ the length of the edge and $\bar{t}_i$ the vector perpendicular to the edge with length $\bar{l}_i$ facing outwards the triangle.

Next we define our bending energy based on this operator. We describe our strain energy density function using Hooke's law as

$$\psi^e_{\text{bending}} = \frac{1}{2} \int_{-\frac{h}{2}}^{\frac{h}{2}} \epsilon_{\text{bending}}(z)^T \boldsymbol{D}^e \epsilon_{\text{bending}}(z) dz, \tag{5}$$

where $\boldsymbol{D}^e = (1-\rho^e)\boldsymbol{D}_{\text{fabric}} + \rho^e \boldsymbol{D}_{\text{reinforcement}}$ is the 3×3 stiffness tensor expressed in Voigt notation, with $\boldsymbol{D}_{\text{fabric}}$ and $\boldsymbol{D}_{\text{reinforcement}}$ the tensors representative of the linear regime of both materials respectively, and

$$\epsilon_{\text{bending}}(z) = (-z\Lambda^e_{xx}, -z\Lambda^e_{yy}, -2z\Lambda^e_{xy})^T \tag{6}$$

is the strain induced by curvature along the thickness of the material z. The energy density is integrated across the thickness of the material h.

Pressurization. We model pressure energy using the ideal gas assumption

$$E_{\text{inflation}} = -PV, \tag{7}$$

where P is a given pressure and V the volume enclosed by the robotic skin.

Force equilibrium. The total energy of the pressurized shell is given by

$$E(\mathbf{x}, \boldsymbol{\rho}) = h \sum_e \bar{A}_e \psi^e_{\text{stretch}} + \sum_e \bar{A}_e \psi^e_{\text{bending}} + E_{\text{inflation}}. \tag{8}$$

The forces of the shell are computed as the negative gradient of this energy with respect to the deformed nodal positions as

$$\boldsymbol{f}(\boldsymbol{x}) = -\frac{\partial E}{\partial \boldsymbol{x}}. \tag{9}$$

The system is at force equilibrium when $\boldsymbol{f}(\boldsymbol{x}) = 0$. Therefore, we find the nodal positions for which the equilibrium configuration is satisfied ($\boldsymbol{x}^{\text{eq}}$) as the solution to the energy minimization problem

$$\boldsymbol{x}^{\text{eq}} = \arg\min_{\boldsymbol{x}} E(\boldsymbol{x}), \tag{10}$$

which we solve using Newton's method with diagonal regularization [Nocedal and Wright 2006].

3.2 Three-Field Topology Optimization

Based on our simulation framework, we build an optimization model to find optimal reinforcement patterns that lead to an ideal approximation of the target shape. Finding optimal distributions of reinforcement material on a textile substrate is a challenging problem. Differentiable topology optimization methods such as SIMP create patterns of material with intermediate densities that are not meaningful from a physical point of view, i.e., they cannot be manufactured. Additionally, we must take into account manufacturability constraints that rise from our fabrication process. Reinforcements that are too thin or small may break or delaminate under actuation. To address these issues, we turn to a three-field topology optimization approach [Zhou et al. 2015]. This approach eliminates intermediate densities and enforces manufacturability constraints through convolutional filters and a novel regularizer that encourages compact designs.

Three-field filtering. We begin by laying out the three-field filtering approach. Given a field of design densities $\boldsymbol{\rho}$, we obtain a smoothed field by applying a filter per element i as

$$\tilde{\rho}_i = \frac{\sum_{j\in N_i} \omega(\bar{\mathbf{x}}_i, \bar{\mathbf{x}}_j)\bar{A}_j\rho_j}{\sum_{j\in N_i} \omega(\bar{\mathbf{x}}_i, \bar{\mathbf{x}}_j)\bar{A}_j}, \tag{11}$$

where $\omega(\bar{\mathbf{x}}_i, \bar{\mathbf{x}}_j) = R - \|\bar{\mathbf{x}}_i - \bar{\mathbf{x}}_j\|$ for $\|\bar{\mathbf{x}}_i - \bar{\mathbf{x}}_j\| \leq R$ and 0 otherwise is a locally supported weighting function describing a neighborhood of elements j for $\bar{\mathbf{x}}_i$ within a radius R, and $\bar{A}_i$ is the area of the element. The purpose of this filter is to enforce a minimum width R for reinforcements by smoothing densities within the given radius. In our experiments we choose $R = 0.6$mm.

Since values for these densities are not binary, they are further processed by a smooth Heaviside filter,

$$\bar{\rho}_i = \frac{\tanh(\beta\eta) + \tanh(\beta(\tilde{\rho}_i - \eta))}{\tanh(\beta\eta) + \tanh(\beta(1-\eta))}, \tag{12}$$

which projects the smoothed density field $\tilde{\boldsymbol{\rho}}$ to a quasi-binary distribution. In this expression, β is a smoothing coefficient for the Heaviside function and η describes the cut-off value between the two materials. We set these parameters to $\beta = 20$ and $\eta = 0.5$ for all experiments. It should be noted that this filter alone does not guarantee entirely binary distributions, as the Heaviside function must be smooth enough to allow differentiability.

The design field $\boldsymbol{\rho}$ together with the two filtered fields $\tilde{\boldsymbol{\rho}}$ and $\bar{\boldsymbol{\rho}}$ compose the three-field topology optimization approach (Fig. 4).

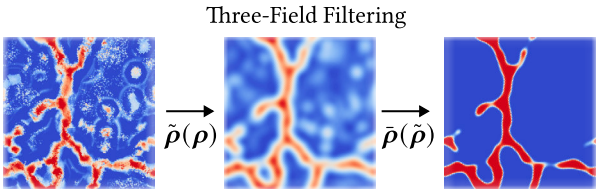

Fig. 4. The three-field filtering approach is composed of an input density field $\boldsymbol{\rho}$, a smoothed field $\tilde{\boldsymbol{\rho}}$ and a Heaviside projected field $\bar{\boldsymbol{\rho}}$.

Density Constraints. In order to obtain strictly binary distributions from these fields, Zhou et al. [2015] propose the following constraints:

$$g_r = \frac{1}{\sum_i \bar{A}_i} \sum_i \bar{A}_i I_i^r \left[\min(\tilde{\rho}_i - \eta_r, 0)\right]^2 < \epsilon \text{ and} \tag{13}$$

$$g_t = \frac{1}{\sum_i \bar{A}_i} \sum_i \bar{A}_i I_i^t \left[\min(\eta_t - \tilde{\rho}_i, 0)\right]^2 < \epsilon, \tag{14}$$

where $I_i^t = \bar{\rho}\exp(-c\|\nabla\tilde{\rho}\|^2)$ and $I_i^r = (1-\bar{\rho})\exp(-c\|\nabla\tilde{\rho}\|^2)$ are locally-supported descriptors that quantify how drastically the smoothed densities $\tilde{\boldsymbol{\rho}}$ change spatially, weighted by their current projected value, where the parameter c controls the length of window. The purpose of this approach is to ensure that densities are not arbitrarily distributed between 0 and 1. Specifically, we ask that no fill ratio is within the range $[\eta_t, \eta_r]$. For concreteness, using thresholds $\eta_t = 0.3$ and $\eta_r = 0.7$ will lead to density values for which material assignment is unambiguous. Without these constraints, density values close to 0.5 (or η) could still arise and material assignments for such values are all but arbitrary. Due to numerical errors introduced by the use of discrete elements, these constraints can not be strictly enforced to be 0. As a consequence, they are framed as inequality constraints with $\epsilon = 10^{-3}$. In our experiments, the value of $c = 100$ produced satisfying results.

Perimeter Regularizer. The three-field filtering approach together with the density constraints guarantee minimum-width reinforcements patterns with binary material distributions. However, in our initial experiments, we observed that the standard version of this algorithm tends to produce small regions (*islands* or *dots*) of isolated material. Whereas such disconnected components do not appear in gravity-regularized problems that seek filled-void material assignments, our fabric-reinforcement material distributions are prone to such artefacts. While these islands can improve the design objective nominally, they generally do not improve functionality and impede clean manufacturing. To discourage these artefacts, we propose a new regularizer that penalizes the total perimeter of the reinforcement (Fig. 5).

We compute the perimeter of the reinforcement material by eroding the projected densities $\bar{\boldsymbol{\rho}}$ using a smooth-minimum filter as

$$F(\bar{\rho}_i) = 1 - \frac{1}{w}\log\left(\frac{1}{n}\sum_{j\in\mathcal{E}}^{n} \exp[w(1-\bar{\rho}_j)]\right), \tag{15}$$

where $\mathcal{E}$ are densities in the convolution window of $\bar{\rho}_i$ and w is a smoothing parameter. Larger values of w result in better approximations of the min function but decrease smoothness and thus affect

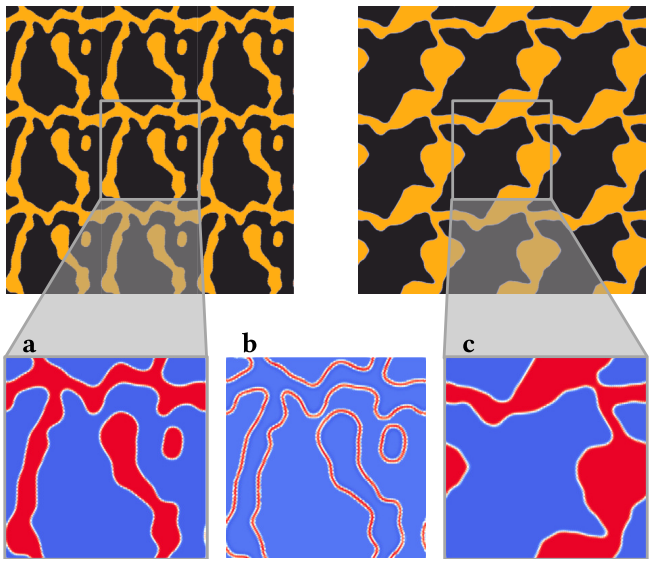

Fig. 5. Our perimeter penalty encourages compact distributions of reinforcement material. We show optimized densities without perimeter penalization (*a*), the corresponding density field used to compute the perimeter (*b*), and the optimization with perimeter penalization (*c*).

the stability of simulation derivatives. We obtained satisfying results by using $w = 0.5$ in our examples. Visually, the operation described by Eq. (15) first inflates the current density field, then subtracts if from the result to obtain a contouring field (Fig. 5b). Summing up all values in the resulting field yields an estimate for the boundary length of the reinforcement material. The per-element perimeter field is given by $P(\bar{\rho}_i) = \bar{\rho}_i - F(\bar{\rho}_i)$ and the regularizer is the sum of the contribution of all elements,

$$R_{\text{perimeter}} = \sum_i P(\bar{\rho}_i) \, . \tag{16}$$

Objective Minimization. We evaluate the performance of a given design $\boldsymbol{\rho}$ using a simple L_2 objective that measures the distance between the simulated static equilibrium $\mathbf{x}^{\text{eq}}$ and the target shape $\mathbf{x}_{\text{target}}$ as

$$T(\mathbf{x}(\boldsymbol{\rho}), \boldsymbol{\rho}) = \frac{1}{2} \|\mathbf{x}^{\text{eq}}(\boldsymbol{\rho}) - \mathbf{x}_{\text{target}}\|^2 \, . \tag{17}$$

With this objective, we define our optimization problem as

$$\begin{aligned} \hat{\boldsymbol{\rho}} = \arg\min_{\boldsymbol{\rho}} \, & T(\boldsymbol{x}(\boldsymbol{\rho}), \boldsymbol{\rho}) + R_{\text{perimeter}} \text{ s.t.} \\ & 0 \leq \rho_i \leq 1, \\ & \boldsymbol{f}(\boldsymbol{x}(\boldsymbol{\rho})) = \mathbf{0}, \\ & g_r(\boldsymbol{\rho}) \leq \varepsilon \text{ and } g_t(\boldsymbol{\rho}) \leq \varepsilon \, . \end{aligned} \tag{18}$$

We find solutions to this minimization problem via the gradient-based method of moving asymptotes (MMA) [Svanberg 1995]. The gradient of the objective T with respect to the design parameters $\boldsymbol{\rho}$ is given by

$$\frac{\mathrm{d}T}{\mathrm{d}\boldsymbol{\rho}} = \frac{\partial \tilde{\boldsymbol{\rho}}}{\partial \boldsymbol{\rho}}^T \frac{\partial \bar{\boldsymbol{\rho}}}{\partial \tilde{\boldsymbol{\rho}}}^T \left(\frac{\partial T}{\partial \bar{\boldsymbol{\rho}}} + \frac{\partial \boldsymbol{x}}{\partial \bar{\boldsymbol{\rho}}}^T \frac{\partial T}{\partial \boldsymbol{x}} \right) , \tag{19}$$

where $\mathbf{x}(\boldsymbol{\rho})$ is computed using sensitivity analysis. The gradient is computed efficiently using the adjoint method. The constraints g_r and g_t are automatically enforced by MMA.

Target Meshes. All of our actuators are designed as developable 3D meshes, from which the flat panels are automatically generated using a planar parameterization method such as ABF++ [Sheffer et al. 2005]. The target mesh is then generated by manually deforming the 3D mesh. In this way, the target mesh shares the same connectivity to the pressurized shell.

4 RESULTS

We evaluate our method on set of examples that include simple fabrication modulation tasks and designs of pneumatic actuators that can bend, twist and compress. We furthermore demonstrate potential use cases by designing a pneumatic crawler and a soft robotic gripper.

4.1 Manufacturing

Our method augments textiles with 3D-printed reinforcements. This approach is compatible with a wide range of filament and textile materials. For actuation, we use generic pneumatic bladders than can be fabricated using standard silicone techniques. To ensure robust and clean manufacturing, islands and other small features must be avoided. To this end, we impose a minimum reinforcement width of 0.6 mm and print with a 0.4 mm nozzle.

Fabrication. Soft robots and actuators were made using a 5 step manufacturing process (Fig. 6). First, the robotic skin design is generated (Fig. 6a) taking into account fabrication constraints. Then, reinforcement patterns are directly 3D printed on soft stretchable fabric (Fig. 6b). The printed design is then cut and sewn (Fig. 6c) into the desired 3D shape of the soft actuator. Meanwhile, the pneumatic bladder for the actuator is fabricated by casting silicone into the desired shape, with tubing and sealing added (Fig. 6d). Finally, the robotic skin is dressed onto the pneumatic bladder and fixed at the extremities using sewing thread (Fig. 6e). The same process was used for fabricating all actuators and robots.

Materials. Robotic skins were made of stretchable jersey (no. 72326, 86% Polyamide, 14% Elasthane) from ExtremTextil. Reinforcements use TPU 95A filament from 3Djake. A Prusa MK3S+ 3D printer was used with the Prusa slicer v2.5. Robotic skin parts were assembled using a standard sewing machine configured in a 4mm zig-zag stitch and using standard cotton thread. Bladders were made by stacking $500\mu m$ thick layers of Dragon skin 20 silicone from Smooth-On. Devices are actuated using a medium sized FlowIO platform [Shtarbanov 2021]. Pneumatic connections and robotic feet were made of standard PLA filament from 3Djake and silicone tubing and glue.

4.2 Characterization

A custom pull tester setup was use to characterize the fabric from 2D samples. It uses a linear rail with a closed loop stepper motor NEMA 17, controlled using a CNC shield and an Arduino UNO with GRBL installed. Forces were measured using a DYLY-109 0 – 5kg force sensor connected to a strain gauge amplifier HX711 and an Arduino

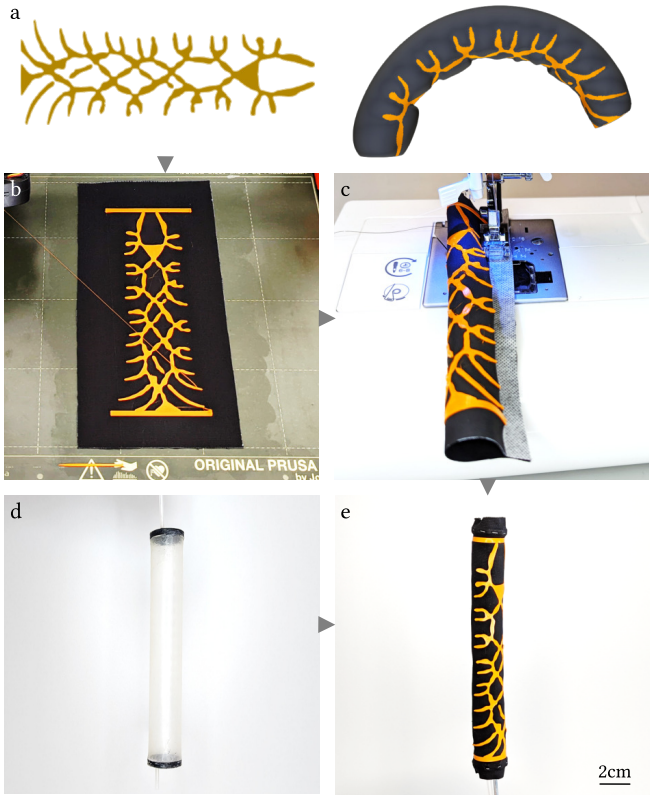

Fig. 6. Design (*a*) and manufacturing process (*b*) of 3D printed TPU reinforcements on stretchable textile substrates to create a cylindrical robotic skin (*c*). The manufactured skin is mounted onto a tubular silicone bladder (*d*) to serve as a pneumatic actuator (*e*) that bends under inflation.

UNO. Pneumatic actuator and robot movements were tracked by video recording in front of a 1cm pitch grid background.

4.3 Mechanical Modulation of Fabric

Our model generates designs that produce desired large deformations by locally modulating the properties of a base material. To validate our model, we design reinforcement patterns that produce desired macromechanical properties. To this end, we consider a square patch of fabric with side lengths of 1cm. In order for this patch to be tileable, we impose periodic boundary conditions on both reinforcement and displacement DoFs during optimization. We targeted 2 anisotropic profiles: the first orthotropic and the second tetragonal, both at 10% strain. The orthotropic tile generated by the model (Fig. 7b) contains geometrical patterns resembling two wavy lines intersecting at 90°. Samples made of 50 tiles were manufactured to experimentally verify the mechanical properties of the design depending on the orientation. Following the simulation model, the fabricated sample exhibits orthotropic behavior (Fig. 7b). Despite an offset, the measured values still show acceptable trend and accuracy. Experimental characterization results for the tetragonal tile (Fig. 7c) show acceptable agreement with the simulation. In summary, the results of these experiments suggest that our approach is able to

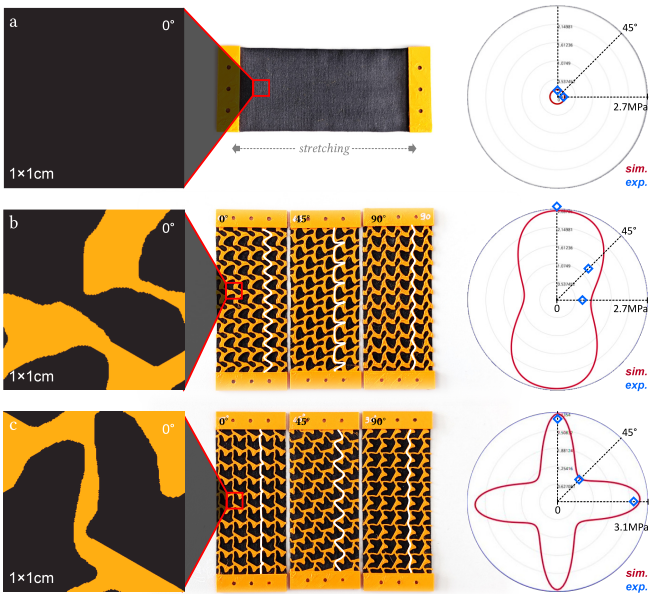

Fig. 7. Design and characterization of fabric reinforcement patterns. (*a*) A blank textile substrate exhibits an isotropic stiffness profile for uniaxial stretching. (*b*) Optimized orthotropic patterns modify the textile stiffness (blue) at 10 % strain depending on direction and show qualitative agreement with the target behavior (red). (*c*) The optimized pattern achieves a direction-dependent stiffness at 0°, 45° and 90° and 10 % strain (blue), showing good agreement with the tetragonal target profile (red).

predict the high-level mechanical response of reinforced fabrics, and to automatically design reinforcement layouts that lead to desired mechanical behavior. This ability is a prerequisite for designing robotic skins for soft robots, which we investigate next.

4.4 Programmable Pneumatic Actuators

We use our method to design a set of robotic skins that, when mounted onto a plain silicon actuator, produce desired deformations upon inflation. As the initial shape, we designed a 15 cm long 2 cm diameter straight cylinder for the pneumatic actuator (Fig. 8a). We used an ultra-thin silicone bladder with negligible stiffness compared to the textile material. We first inflated the actuator without reinforcement. As expected, it inflates into a straight tubular shape, increasing in diameter and length. This behavior is also observed in simulation. As a proof of concept, we programmed different deformations for the same base actuator. First, we prescribe a target shape corresponding to a constant-curvature bend of 180° (Fig. 8b). Our method finds a reinforcement pattern that achieves this target at a pressure of 5kPa in simulation. Experimentally, the manufactured actuator generated the same motion, but lagging behind the simulation, bending up to a maximum of 150° at a pressure of 13kPa. Remarkably, the resulting pattern differs from most human-designed actuators, which tend to use straight-line reinforcements [Elmoughni et al. 2021; Luo et al. 2022; Yap et al. 2017]. In contrast, our model generated hollow, diamond-shaped reinforcement structures on the inner side, with ribs extending upward.

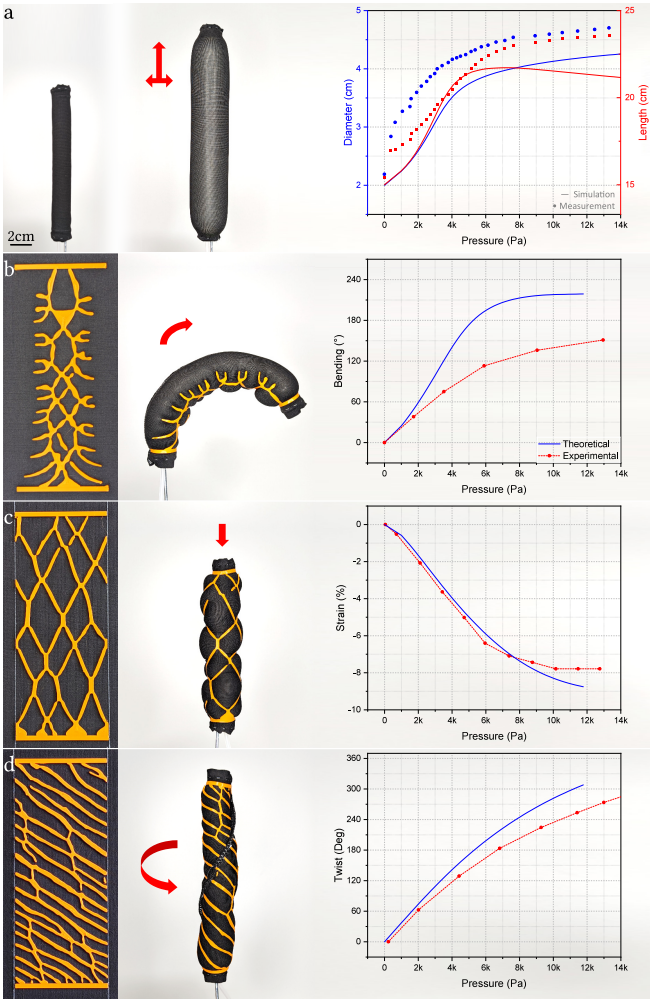

Fig. 8. Evaluation of reinforced pneumatic actuators. (*a*) Inflation of a 2×15 cm cylindrical balloon without reinforcement. Simulation and measurement predict that its diameter and length increase under low pressure and then saturate above 10kPa. (*b*) Bending, (*c*)) contracting, and (*d*) twisting actuators once inflated. Simulated and measured deformations are shown on the right.

As a second experiment in this series, we designed a robotic skin that produces an axial contraction upon actuation (Fig. 8c). The optimized reinforcement pattern exhibits two sets of parallel lines, crossing at an angle between 60 and 70 which is conceptually similar to McKibben pneumatic artificial muscles [Al-Ibadi et al. 2017; Aliseichik et al. 2022; Daerden et al. 2002].

We asked for a contraction of 8%. The physical prototype achieves 7.8% contraction at a pressure of 10kPa. For a third experiment, we prescribe a twisting deformation as the target shape (Fig. 8d). Our algorithm finds a pattern that is composed mainly of tilted stripes. This pattern is similar to existing twisting actuators [Chen et al. 2021b; Connolly et al. 2017; Nguyen and Zhang 2020; Schaffner et al. 2018], but with some vertical connections between the tilted lines that restrict its elongation under inflation. Experimentally, the

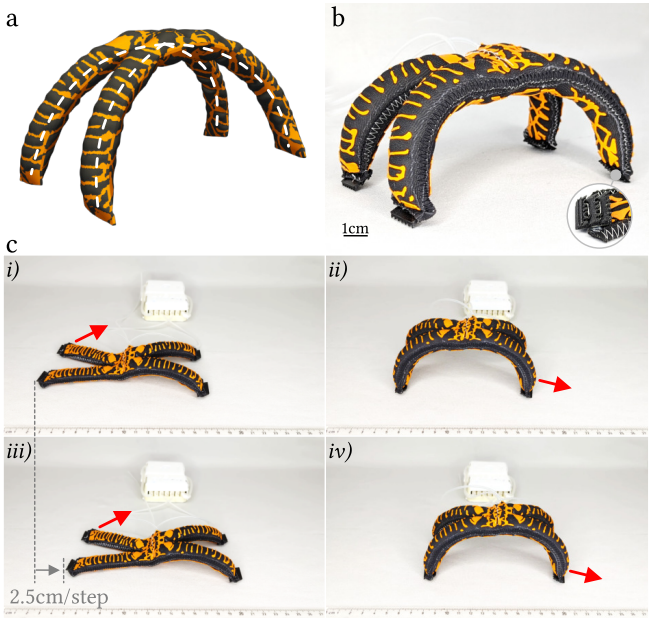

Fig. 9. Pneumatic walker. Our method generates a design that enables the inflated robot to stand in simulation (*a*). The physical prototype qualitatively tracks the simulated deformation (*b*). Actuating the three chambers of the robot in coordination leads to successful locomotion (*c*) with forward motion of approximately 2.5cm per cycle (*i-ii* and *iii-iv* showing two subsequent cycles, respectively).

fabricated actuator twists by 300° at a pressure of 15 kPa, lagging slightly behind the predicted behavior in simulation.

In summary, these results suggest that our method is able to design robotic skins that qualitatively track the behavior of prescribed basic actuation tasks. The patterns computed by our algorithm are geometrically complex and exploit the design freedom offered by digital manufacturing.

4.5 Soft robot skin

To illustrate the potential of our method for generating design with more complex functions, we design a quadruped walking robot [Morin et al. 2012; Shepherd et al. 2011; Tolley et al. 2014] and a three fingered gripper [Ilievski et al. 2011; Lee et al. 2017; Shintake et al. 2018]. For the soft robotic walker, we start from an *X*-shaped layout and ask that its legs should bend to 90° at 20kPa (Fig. 9b). Due to the symmetry of the prescribed motion, we optimize for one leg. Similar to our bending actuator (Fig. 8b), the resulting design show hollow, diamond-shaped reinforcement structures below the limbs and ribs extending upward. The middle part of the walker, joining the four legs, is covered with large areas of reinforcement such as to contain its inflation and stiffen its structure. A bladder with three individually controlled chambers was used for pneumatic actuation, one for the front limbs, back limbs and the middle body. Finally, we added unidirectional nonslip feet to improve grip. As best seen in the accompanying video, the manufactured robot was able to move forward at a speed of 2.5cm per actuation cycle (Fig. 9c).

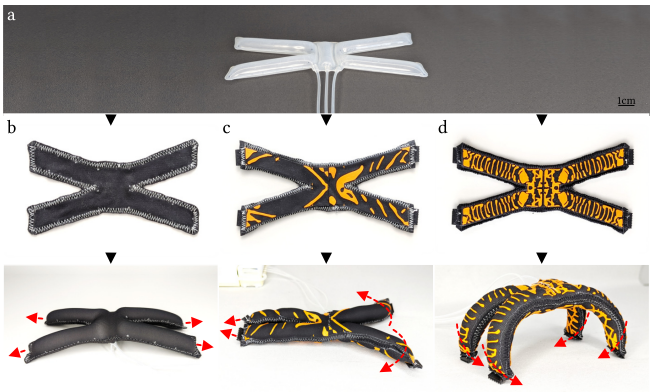

Fig. 10. A flat four legged pneumatic bladder (*a*) can perform different motions upon inflation depending on its robotic skin. Without reinforcement (*b*) the soft robot lays flat. With a crawling reinforcement pattern (*c*) the robot crawls. And with a standing reinforcement pattern (*d*) the robot can stand up on its legs.

As shown in Fig. 10, our method offers flexibility to design robots for various applications or obstacles. For example, a soft swimmer may need to perform a specific stroke (Fig. 10c), which can be employed as a target shape to our method to adapt the design.

The model can also design grippers (Fig. 1c), a highly demanded task in soft robotics. In this context, a key advantage of our automated design approach is that it can easily adapt the gripper to grasp objects of different sizes, shapes and stiffness.

5 CONCLUSIONS

We presented ToRoS, a new method to automatically design robotic skins reinforced with strain limiting patterns to control the motion of soft pneumatic robots. Our approach enables us to explore and take advantage of new design spaces offered by 3D printing. To automatically generate designs that optimally approximate target behaviors, we have addressed several key challenges. First, we developed a manufacturing process that enable us to fabricate modular soft robots using standard filament-based 3D printers. Second, to explore this new design space, we developed a computational method that automatically designs optimized robotic skins, taking into account fabrication constraints. Lastly, we improve on an existing three-field topology optimization scheme to encourage fully connected reinforcement layouts using a novel regularization term. Our experimental results illustrate the potential of our method for designing functional soft robots on demand, and to adapt them to new scenarios using simple deformation targets.

5.1 Simulation Accuracy

Our simulation framework is able to predict the high-level behavior of the manufactured devices but achieving numerical agreement between simulation and physical experiments remains a challenge. This is in part due to the fact that our pressurized actuators undergo extreme deformations, leading to highly nonlinear stress-strain responses. Furthermore, we model textiles as perfectly isotropic and elastic materials. Real-world textiles exhibit anisotropy and plasticity, which are not accounted for by our model. Additional simplifications made in our simulation framework include the assumption of perfect bonding of fabric and reinforcement as well as the lack of a friction model between the silicone bladder and the robotic skin. While all these aspects affect the nominal accuracy of our simulations, our model nevertheless predict the overall performance of our manufactured designs sufficiently well.

5.2 Limitations and Future Work

The current computational model generates reinforcements using only one flexible material. Nevertheless, using additional material for reinforcements would enable better control over deformation. More complex targets could be achieved by combining several reinforcement materials having different properties. We also imagine in future that more complex structures with specific properties could be added onto robotic skin like compliant mechanisms and metamaterials [Fan et al. 2021; Schumacher et al. 2018]. While we have demonstrated basic locomotion capabilities for our soft robots, the control signals were programmed manually. In the future, it would be interesting to co-design robotic skins and control algorithms.

6 ACKNOWLEDGEMENTS

We are grateful to the anonymous reviewers for their valuable comments. This work was supported by the European Research Council (ERC) under the European Union's Horizon 2020 research and innovation program (grant agreement No. 866480), and the Swiss National Science Foundation through SNF project grant 200021_200644.

REFERENCES

Alaa Al-Ibadi, Samia Nefti-Meziani, and Steve Davis. 2017. Efficient Structure-Based Models for the McKibben Contraction Pneumatic Muscle Actuator: The Full Description of the Behaviour of the Contraction PMA. *Actuators* 6, 4 (oct 2017), 32. https://doi.org/10.3390/act6040032

A. P. Aliseichik, D. A. Gribkov, A. R. Efimov, I. A. Orlov, V. E. Pavlovsky, A. V. Podoprosvetov, and I. V. Khaidukova. 2022. Artificial Muscles (Review Article). *Journal of Computer and Systems Sciences International* 61, 2 (apr 2022), 270–293. https://doi.org/10.1134/S1064230722010026

Grégoire Allaire, Frédéric De Gournay, François Jouve, and Anca-Maria Toader. 2005. Structural optimization using topological and shape sensitivity via a level set method. *Control and cybernetics* 34, 1 (2005), 59.

Grégoire Allaire, François Jouve, and Anca-Maria Toader. 2004. Structural optimization using sensitivity analysis and a level-set method. *Journal of computational physics* 194, 1 (2004), 363–393.

Erik Andreassen, Anders Clausen, Mattias Schevenels, Boyan S Lazarov, and Ole Sigmund. 2011. Efficient topology optimization in MATLAB using 88 lines of code. *Structural and Multidisciplinary Optimization* 43, 1 (2011), 1–16.

Melanie Baumgartner, Florian Hartmann, Michael Drack, David Preninger, Daniela Wirthl, Robert Gerstmayr, Lukas Lehner, Guoyong Mao, Roland Pruckner, Stepan Demchyshyn, et al. 2020. Resilient yet entirely degradable gelatin-based biogels for soft robots and electronics. *Nature Materials* 19, 10 (2020), 1102–1109.

Martin P Bendsøe and Ole Sigmund. 1995. *Optimization of structural topology, shape, and material*. Vol. 414. Springer.

Martin Philip Bendsoe and Ole Sigmund. 2013. *Topology optimization: theory, methods, and applications*. Springer Science & Business Media.

James M. Bern, Kai-Hung Chang, and Stelian Coros. 2017. Interactive Design of Animated Plushies. *ACM Trans. Graph.* 36, 4, Article 80 (jul 2017), 11 pages. https://doi.org/10.1145/3072959.3073700

Bernd Bickel, Moritz Bächer, Miguel A Otaduy, Hyunho Richard Lee, Hanspeter Pfister, Markus Gross, and Wojciech Matusik. 2010. Design and fabrication of materials with desired deformation behavior. *ACM Transactions on Graphics (TOG)* 29, 4 (2010), 1–10.

Joshua Bishop-Moser, Girish Krishnan, Charles Kim, and Sridhar Kota. 2012. Design of soft robotic actuators using fluid-filled fiber-reinforced elastomeric enclosures

in parallel combinations. In *IEEE International Conference on Intelligent Robots and Systems*. IEEE, 4264–4269. https://doi.org/10.1109/IROS.2012.6385966

Joran W. Booth, Dylan Shah, Jennifer C. Case, Edward L. White, Michelle C. Yuen, Olivier Cyr-Choiniere, and Rebecca Kramer-Bottiglio. 2018. OmniSkins: Robotic skins that turn inanimate objects into multifunctional robots. *Science Robotics* 3, 22 (2018), eaat1853. https://doi.org/10.1126/scirobotics.aat1853 arXiv:https://www.science.org/doi/pdf/10.1126/scirobotics.aat1853

Callie Branyan, Ahmad Rafsanjani, Katia Bertoldi, Ross L. Hatton, and Yigit Mengüç. 2022. Curvilinear Kirigami Skins Let Soft Bending Actuators Slither Faster. *Frontiers in Robotics and AI* 9 (2022), 872007.

Trevor L. Buckner, R. Adam Bilodeau, Sang Yup Kim, and Rebecca Kramer-Bottiglio. 2020. Roboticizing fabric by integrating functional fibers. *Proceedings of the National Academy of Sciences* 117, 41 (2020), 25360–25369. https://doi.org/10.1073/pnas.2006211117 arXiv:https://www.pnas.org/doi/pdf/10.1073/pnas.2006211117

Oisín Byrne, Fergal Coulter, Mark Glynn, James F.X. Jones, Aisling Ní Annaidh, Eoin D. O'Cearbhaill, and Dónal P. Holland. 2018. Additive manufacture of composite soft pneumatic actuators. *Soft Robotics* 5, 6 (2018), 726–736. https://doi.org/10.1089/soro.2018.0030

Brandon Caasenbrood, Alexander Pogromsky, and Henk Nijmeijer. 2020. A Computational Design Framework for Pressure-driven Soft Robots through Nonlinear Topology Optimization. In *2020 3rd IEEE International Conference on Soft Robotics, RoboSoft 2020*. IEEE, 633–638. https://doi.org/10.1109/RoboSoft48309.2020.9116010

Jennifer C. Case, Michelle C. Yuen, Jane Jacobs, and Rebecca Kramer-Bottiglio. 2019. Robotic Skins That Learn to Control Passive Structures. *IEEE Robotics and Automation Letters* 4, 3 (2019), 2485–2492. https://doi.org/10.1109/LRA.2019.2906552

Shitong Chen, Feifei Chen, Zizheng Cao, Yusheng Wang, Yunpeng Miao, Guoying Gu, and Xiangyang Zhu. 2021a. Topology Optimization of Skeleton-Reinforced Soft Pneumatic Actuators for Desired Motions. *IEEE/ASME Transactions on Mechatronics* 26, 4 (aug 2021), 1745–1753. https://doi.org/10.1109/TMECH.2021.3071394

Shitong Chen, Feifei Chen, Zizheng Cao, Yusheng Wang, Yunpeng Miao, Guoying Gu, and Xiangyang Zhu. 2021b. Topology Optimization of Skeleton-Reinforced Soft Pneumatic Actuators for Desired Motions. *IEEE/ASME Transactions on Mechatronics* 26, 4 (2021), 1745–1753. https://doi.org/10.1109/TMECH.2021.3071394

Fionnuala Connolly, Conor J. Walsh, and Katia Bertoldi. 2017. Automatic design of fiber-reinforced soft actuators for trajectory matching. *Proceedings of the National Academy of Sciences of the United States of America* 114, 1 (jan 2017), 51–56. https://doi.org/10.1073/pnas.1615140114

Fergal B. Coulter and Anton Ianakiev. 2015. 4D Printing Inflatable Silicone Structures. *3D Printing and Additive Manufacturing* 2, 3 (2015), 140–144. https://doi.org/10.1089/3dp.2015.0017

Frank Daerden, Frank Daerden, and Dirk Lefeber. 2002. Pneumatic artificial muscles: Actuators for robotics and automation. *European Journal of Mechanical and Environmental Engineering* 47, 1 (2002), 11–21. http://citeseerx.ist.psu.edu/viewdoc/summary?doi=10.1.1.89.6717

Nazek El-Atab, Rishabh B. Mishra, Fhad Al-Modaf, Lana Joharji, Aljohara A. Alsharif, Haneen Alamoudi, Marlon Diaz, Nadeem Qaiser, and Muhammad Mustafa Hussain. 2020. Soft Actuators for Soft Robotic Applications: A Review. *Advanced Intelligent Systems* 2, 10 (2020), 2000128. https://doi.org/10.1002/aisy.202000128 arXiv:https://onlinelibrary.wiley.com/doi/pdf/10.1002/aisy.202000128

Hend M. Elmoughni, Ayse Feyza Yilmaz, Kadir Ozlem, Fidan Khalilbayli, Leonardo Cappello, Asli Tuncay Atalay, Gökhan Ince, and Ozgur Atalay. 2021. Machine-Knitted Seamless Pneumatic Actuators for Soft Robotics: Design, Fabrication, and Characterization. *Actuators* 10, 5 (apr 2021), 94. https://doi.org/10.3390/act10050094

Junxiang Fan, Lei Zhang, Shuaishuai Wei, Zhi Zhang, Seung Kyum Choi, Bo Song, and Yusheng Shi. 2021. A review of additive manufacturing of metamaterials and developing trends. *Materials Today* 50 (nov 2021), 303–328. https://doi.org/10.1016/j.mattod.2021.04.019

A. N. Gent. 1996. A New Constitutive Relation for Rubber. *Rubber Chemistry and Technology* 69, 1 (03 1996), 59–61. https://doi.org/10.5254/1.3538357 arXiv:https://meridian.allenpress.com/rct/article-pdf/69/1/59/1945987/1_3538357.pdf

Eitan Grinspun, Yotam Gingold, Jason Reisman, and Denis Zorin. 2006. Computing discrete shape operators on general meshes. *Computer Graphics Forum* 25, 3 (2006), 547–556. https://doi.org/10.1111/j.1467-8659.2006.00974.x arXiv:https://onlinelibrary.wiley.com/doi/pdf/10.1111/j.1467-8659.2006.00974.x

B. Grossi, H. Palza, J.C. Zagal, C. Falcón, and G. During. 2021. Metarpillar: Soft robotic locomotion based on buckling-driven elastomeric metamaterials. *Materials & Design* 212 (2021), 110285. https://doi.org/10.1016/j.matdes.2021.110285

Shinichi Hirai, Pierre Cusin, Hiroki Tanigawa, Tomohiro Masui, Satoshi Konishi, and Sadao Kawamura. 2000. Qualitative synthesis of deformable cylindrical actuators through constraint topology. In *IEEE International Conference on Intelligent Robots and Systems*, Vol. 1. IEEE, 197–202. https://doi.org/10.1109/IROS.2000.894604

Filip Ilievski, Aaron D. Mazzeo, Robert F. Shepherd, Xin Chen, and George M. Whitesides. 2011. Soft Robotics for Chemists. *Angewandte Chemie* 123, 8 (feb 2011), 1930–1935. https://doi.org/10.1002/ange.201006464

Lishuai Jin, Antonio Elia Forte, Bolei Deng, Ahmad Rafsanjani, and Katia Bertoldi. 2020. Kirigami-Inspired Inflatables with Programmable Shapes. *Advanced Materials* (2020), 2001863.

David Jourdan, Mélina Skouras, Etienne Vouga, and Adrien Bousseau. 2020. Printing-on-Fabric Meta-Material for Self-Shaping Architectural Models. (2020), 1–19.

R Kemmler, A Lipka, and E Ramm. 2005. Large deformations and stability in topology optimization. *Structural and Multidisciplinary Optimization* 30, 6 (2005), 459–476.

Chiwon Lee, Myungjoon Kim, Yoon Jae Kim, Nhayoung Hong, Seungwan Ryu, H. Jin Kim, and Sungwan Kim. 2017. Soft robot review. *International Journal of Control, Automation and Systems* 15, 1 (feb 2017), 3–15. https://doi.org/10.1007/s12555-016-0462-3

Yunfeng Luo, Quhao Li, and Shutian Liu. 2019. Topology optimization of shell–infill structures using an erosion-based interface identification method. *Computer Methods in Applied Mechanics and Engineering* 355 (2019), 94–112. https://doi.org/10.1016/j.cma.2019.05.017

Yiyue Luo, Kui Wu, Andrew Spielberg, Michael Foshey, Daniela Rus, Tomás Palacios, and Wojciech Matusik. 2022. Digital Fabrication of Pneumatic Actuators with Integrated Sensing by Machine Knitting. In *CHI Conference on Human Factors in Computing Systems*. ACM, New York, NY, USA, 1–13. https://doi.org/10.1145/3491102.3517577

Pingchuan Ma, Tao Du, John Z. Zhang, Kui Wu, Andrew Spielberg, Robert K. Katzschmann, and Wojciech Matusik. 2021. DiffAqua: A Differentiable Computational Design Pipeline for Soft Underwater Swimmers with Shape Interpolation. *ACM Trans. Graph.* 40, 4, Article 132 (jul 2021), 14 pages. https://doi.org/10.1145/3450626.3459832

Sehee Min, Jungdam Won, Seunghwan Lee, Jungnam Park, and Jehee Lee. 2019. SoftCon: Simulation and Control of Soft-Bodied Animals with Biomimetic Actuators. *ACM Trans. Graph.* 38, 6, Article 208 (nov 2019), 12 pages. https://doi.org/10.1145/3355089.3356497

Juan Montes, Yinwei Du, Ronan Hinchet, Stelian Coros, and Bernhard Thomaszewski. 2023. Differentiable Stripe Patterns for Inverse Design of Structured Surfaces. *ACM Transactions on Graphics (TOG) (to appear)* 42 (2023). Issue 5. https://doi.org/10.1145/3462758

Stephen A. Morin, Robert F. Shepherd, Sen Wai Kwok, Adam A. Stokes, Alex Nemiroski, and George M. Whitesides. 2012. Camouflage and Display for Soft Machines. *Science* 337, 6096 (aug 2012), 828–832. https://doi.org/10.1126/science.1222149

Bobak Mosadegh, Panagiotis Polygerinos, Christoph Keplinger, Sophia Wennstedt, Robert F Shepherd, Unmukt Gupta, Jongmin Shim, Katia Bertoldi, Conor J Walsh, and George M Whitesides. 2014. Pneumatic networks for soft robotics that actuate rapidly. *Advanced functional materials* 24, 15 (2014), 2163–2170.

Pham Huy Nguyen and Wenlong Zhang. 2020. Design and Computational Modeling of Fabric Soft Pneumatic Actuators for Wearable Assistive Devices. *Scientific Reports* 10, 1 (dec 2020), 9638. https://doi.org/10.1038/s41598-020-65003-2

Jorge Nocedal and Stephen J. Wright. 2006. *Numerical Optimization* (2e ed.). Springer, New York, NY, USA.

Julian Panetta, Florin Isvoranu, Tian Chen, Emmanuel Siéfert, Benoît Roman, and Mark Pauly. 2021. Computational Inverse Design of Surface-Based Inflatables. *ACM Trans. Graph.* 40, 4, Article 40 (jul 2021), 14 pages. https://doi.org/10.1145/3450626.3459789

Julian Panetta, Qingnan Zhou, Luigi Malomo, Nico Pietroni, Paolo Cignoni, and Denis Zorin. 2015. Elastic textures for additive fabrication. *ACM Transactions on Graphics (TOG)* 34, 4 (2015), 1–12.

J. H. Pikul, S. Li, H. Bai, R. T. Hanlon, I. Cohen, and R. F. Shepherd. 2017. Stretchable surfaces with programmable 3D texture morphing for synthetic camouflaging skins. *Science* 358, 6360 (oct 2017), 210–214. https://doi.org/10.1126/science.aan5627

Joshua Pinskier and David Howard. 2022. From Bioinspiration to Computer Generation: Developments in Autonomous Soft Robot Design. *Advanced Intelligent Systems* 4, 1 (2022), 2100086. https://doi.org/10.1002/aisy.202100086 arXiv:https://onlinelibrary.wiley.com/doi/pdf/10.1002/aisy.202100086

Daniela Rus and Michael T Tolley. 2015. Design, fabrication and control of soft robots. *Nature* 521, 7553 (2015), 467–475.

Manuel Schaffner, Jakob A. Faber, Lucas Pianegonda, Patrick A. Rühs, Fergal Coulter, and André R. Studart. 2018. 3D printing of robotic soft actuators with programmable bioinspired architectures. *Nature Communications* 9, 1 (dec 2018), 878. https://doi.org/10.1038/s41467-018-03216-w

François Schmitt, Olivier Piccin, Laurent Barbé, and Bernard Bayle. 2018. Soft robots manufacturing: A review. *Frontiers Robotics AI* 5, JUN (jul 2018). https://doi.org/10.3389/frobt.2018.00084

Christian Schumacher, Bernd Bickel, Jan Rys, Steve Marschner, Chiara Daraio, and Markus Gross. 2015. Microstructures to control elasticity in 3D printing. *ACM Transactions on Graphics (Tog)* 34, 4 (2015), 1–13.

Christian Schumacher, Steve Marschner, Markus Gross, and Bernhard Thomaszewski. 2018. Mechanical characterization of structured sheet materials. *ACM Transactions on Graphics (TOG)* 37, 4 (2018), 1–15.

Dylan Shah, Bilige Yang, Sam Kriegman, Michael Levin, Josh Bongard, and Rebecca Kramer-Bottiglio. 2021. Shape Changing Robots: Bioinspiration, Simulation, and Physical Realization. *Advanced Materials* 33, 19 (2021), 2002882. https://doi.org/10.1002/adma.202002882 arXiv:https://onlinelibrary.wiley.com/doi/pdf/10.1002/adma.202002882

Alla Sheffer, Bruno Lévy, Maxim Mogilnitsky, and Alexander Bogomyakov. 2005. ABF++: Fast and Robust Angle Based Flattening. *ACM Trans. Graph.* 24, 2 (apr 2005), 311–330. https://doi.org/10.1145/1061347.1061354

Robert F. Shepherd, Filip Ilievski, Wonjae Choi, Stephen A. Morin, Adam A. Stokes, Aaron D. Mazzeo, Xin Chen, Michael Wang, and George M. Whitesides. 2011. Multigait soft robot. *Proceedings of the National Academy of Sciences* 108, 51 (2011), 20400–20403. https://doi.org/10.1073/pnas.1116564108 arXiv:https://www.pnas.org/doi/pdf/10.1073/pnas.1116564108

Jun Shintake, Vito Cacucciolo, Dario Floreano, and Herbert Shea. 2018. Soft Robotic Grippers. *Advanced Materials* 30, 29 (jul 2018), 1707035. https://doi.org/10.1002/adma.201707035

Ali Shtarbanov. 2021. FlowIO Development Platform – the Pneumatic "Raspberry Pi" for Soft Robotics. In *Extended Abstracts of the 2021 CHI Conference on Human Factors in Computing Systems*. ACM, New York, NY, USA, 1–6. https://doi.org/10.1145/3411763.3451513

Ole Sigmund. 2007. Morphology-based black and white filters for topology optimization. *Structural and Multidisciplinary Optimization* 33 (2007), 401–424. https://api.semanticscholar.org/CorpusID:122761654

Mélina Skouras, Bernhard Thomaszewski, Bernd Bickel, and Markus Gross. 2012. Computational design of rubber balloons. *Computer Graphics Forum* 31, 2 (may 2012), 835–844. https://doi.org/10.1111/j.1467-8659.2012.03064.x

Mélina Skouras, Bernhard Thomaszewski, Peter Kaufmann, Akash Garg, Bernd Bickel, Eitan Grinspun, and Markus Gross. 2014. Designing inflatable structures. *ACM Transactions on Graphics (TOG)* 33, 4 (2014), 1–10.

Yi Sun, Yun Seong Song, and Jamie Paik. 2013. Characterization of silicone rubber based soft pneumatic actuators. In *2013 IEEE/RSJ International Conference on Intelligent Robots and Systems*. Ieee, 4446–4453.

Krister Svanberg. 1995. A globally convergent version of MMA without linesearch. In *Proceedings of the first world congress of structural and multidisciplinary optimization*, Vol. 28. Goslar, Germany, 9–16.

Charbel Tawk and Gursel Alici. 2021. A Review of 3D-Printable Soft Pneumatic Actuators and Sensors: Research Challenges and Opportunities. *Advanced Intelligent Systems* 3, 6 (2021), 2000223. https://doi.org/10.1002/aisy.202000223 arXiv:https://onlinelibrary.wiley.com/doi/pdf/10.1002/aisy.202000223

Michael T. Tolley, Robert F. Shepherd, Bobak Mosadegh, Kevin C. Galloway, Michael Wehner, Michael Karpelson, Robert J. Wood, and George M. Whitesides. 2014. A Resilient, Untethered Soft Robot. *Soft Robotics* 1, 3 (sep 2014), 213–223. https://doi.org/10.1089/soro.2014.0008

Thibault Tricard, Vincent Tavernier, Cédric Zanni, Jonàs Martínez, Pierre-Alexandre Hugron, Fabrice Neyret, and Sylvain Lefebvre. 2020. Freely orientable microstructures for designing deformable 3D prints. *ACM Trans. Graph.* 39, 6 (2020), 211–1.

T. J. Wallin, J. Pikul, and R. F. Shepherd. 2018. 3D printing of soft robotic systems. *Nature Reviews Materials* 3, 6 (jun 2018), 84–100. https://doi.org/10.1038/s41578-018-0002-2

Fengwen Wang, Boyan Stefanov Lazarov, Ole Sigmund, and Jakob Søndergaard Jensen. 2014. Interpolation scheme for fictitious domain techniques and topology optimization of finite strain elastic problems. *Computer Methods in Applied Mechanics and Engineering* 276 (2014), 453–472. https://doi.org/10.1016/j.cma.2014.03.021

Hong Kai Yap, Frederick Sebastian, Christopher Wiedeman, and Chen-Hua Yeow. 2017. Design and characterization of low-cost fabric-based flat pneumatic actuators for soft assistive glove application. In *2017 International Conference on Rehabilitation Robotics (ICORR)*. IEEE, 1465–1470. https://doi.org/10.1109/ICORR.2017.8009454

Osman Dogan Yirmibesoglu, John Morrow, Steph Walker, Walker Gosrich, Reece Canizares, Hansung Kim, Uranbileg Daalkhaijav, Chloe Fleming, Callie Branyan, and Yigit Menguc. 2018. Direct 3D printing of silicone elastomer soft robots and their performance comparison with molded counterparts. In *2018 IEEE International Conference on Soft Robotics (RoboSoft)*. IEEE, 295–302. https://doi.org/10.1109/ROBOSOFT.2018.8404935

Jonas Zehnder, Espen Knoop, Moritz Bächer, and Bernhard Thomaszewski. 2017. Metasilicone: Design and Fabrication of Composite Silicone with Desired Mechanical Properties. *ACM Trans. Graph.* 36, 6, Article 240 (nov 2017), 13 pages. https://doi.org/10.1145/3130800.3130881

Jonas Zehnder, Yue Li, Stelian Coros, and Bernhard Thomaszewski. 2021. NTopo: Mesh-free Topology Optimization using Implicit Neural Representations. In *Advances in Neural Information Processing Systems*, M. Ranzato, A. Beygelzimer, Y. Dauphin, P.S. Liang, and J. Wortman Vaughan (Eds.), Vol. 34. Curran Associates, Inc., 10368–10381. https://proceedings.neurips.cc/paper/2021/file/55d99a37b2e1badba7c8df4ccd506a88-Paper.pdf

Mingdong Zhou, Boyan S. Lazarov, Fengwen Wang, and Ole Sigmund. 2015. Minimum length scale in topology optimization by geometric constraints. *Computer Methods in Applied Mechanics and Engineering* 293 (2015), 266–282. https://doi.org/10.1016/j.cma.2015.05.003

Bo Zhu, Mélina Skouras, Desai Chen, and Wojciech Matusik. 2017. Two-scale topology optimization with microstructures. *ACM Transactions on Graphics (TOG)* 36, 4 (2017), 1.

Jun Zou, Yangqiao Lin, Chen Ji, and Huayong Yang. 2018. A Reconfigurable Omnidirectional Soft Robot Based on Caterpillar Locomotion. *Soft Robotics* 5, 2 (apr 2018), 164–174. https://doi.org/10.1089/soro.2017.0008